BIOCHEMISTRY
including biophysical chemistry & molecular biology

Article

pubs.acs.org/biochemistry

Changes in Apaf-1 Conformation That Drive Apoptosome Assembly

Shujun Yuan,[†] Maya Topf,[‡] Thomas F. Reubold,[§] Susanne Eschenburg,[§] and Christopher W. Akey*[,†]

[†]Department of Physiology and Biophysics, Boston University School of Medicine, 700 Albany Street, Boston, Massachusetts 02118, United States

[‡]Institute of Structural and Molecular Biology, Department of Biological Sciences, Birkbeck, University of London, Malet Street, London WC1E 7HX

[§]Institute for Biophysical Chemistry, Hannover Medical School, 30625 Hannover, Germany

ABSTRACT: Apoptosome assembly is highly regulated in the intrinsic cell death pathway. To better understand this step, we created an improved model of the human apoptosome using a crystal structure of full length Apaf-1 and a single particle, electron density map at ~9.5 Å resolution. The apoptosome model includes N-terminal domains of Apaf-1, cognate β-propellers, and cytochrome *c*. A direct comparison of Apaf-1 in the apoptosome and as a monomer reveals conformational changes that occur during the first two steps of assembly. This includes an induced-fit mechanism for cytochrome *c* binding to regulatory β-propellers, which is dependent on shape and charge complementarity, and a large rotation of the nucleotide binding module during nucleotide exchange. These linked conformational changes create an extended Apaf-1 monomer and drive apoptosome assembly. Moreover, the N-terminal CARD in the inactive Apaf-1 monomer is not shielded from other proteins by β-propellers. Hence, the Apaf-1 CARD may be free to interact with a procaspase-9 CARD either before or during apoptosome assembly. Irrespective of the timing, the end product of assembly is a holo-apoptosome with an acentric CARD−CARD disk and tethered pc-9 catalytic domains. Subsequent activation of pc-9 leads to a proteolytic cascade and cell death.

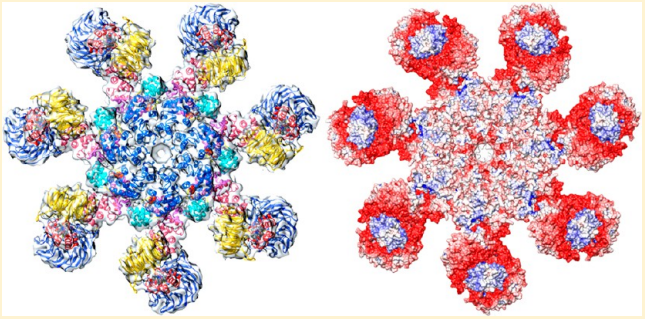

The intrinsic death pathway in metazoans is responsible for terminating infected or inappropriately dividing cells and also removes superfluous or damaged cells during development, tissue homeostasis, stroke, and neurodegeneration.[1−5] In humans, apoptosis protease activating factor 1 (Apaf-1) resides in the cytoplasm of healthy cells in an inactive conformation.[6,7] Pro-death signals result in the release of cytochrome *c* from binding sites on the inner mitochondrial membrane that contain cardiolipin molecules.[8] Cytochrome *c* transits to the cytosol upon permeabilization of the mitochondrial membrane[9] and interacts with Apaf-1, which triggers nucleotide exchange and apoptosome assembly.[6,7,10−12] For Apaf-1, either dATP or ATP can be used during assembly,[10,13−15] but the concentration of the latter NTP is much higher in cells and thus may be more important.[16]

The apoptosome is a heptameric platform that binds and activates procaspase-9 (pc-9) to form the holo-apoptosome.[17−20] The resulting holo-apoptosome is an asymmetric proteolysis machine, which contains a disk comprised of Apaf-1 and pc-9 CARDs that sits on top of the platform in an acentric position.[19,20] The active apoptosome cleaves procaspase-3 and -7 dimers to start a proteolytic cascade that results in cell death.[21−24] Two models have been considered for pc-9 activation. In one model, pc-9 monomers bind to the apoptosome via CARD−CARD interactions, and subsequent dimerization of the zymogens results in activation.[23,25−27] In a second model, pc-9 catalytic domains bind to a site on the apoptosome and become activated in a process that may require either dimers or monomers.[20,23,28] Importantly, both models require a high local concentration of pc-9 molecules in the vicinity of the platform to trigger activation.

A crystal structure was recently determined for the *C. elegans* apoptosome,[29] and models have been obtained by single particle electron cryo-microscopy for *Drosophila* and human apoptosomes.[19,20] To provide a better understanding of apoptosome structure and assembly, we have modeled the human complex using a recent crystal structure of full length mouse Apaf-1,[30] cytochrome *c*, and a previous electron density map of the apoptosome at ~9.5 Å resolution.[19] We then compared structures of ADP and ATP bound conformations of Apaf-1 to highlight changes that occur during assembly. We find that the 7-blade β-propeller undergoes a large rotation to clamp cytochrome *c* between two β-propellers in the regulatory region. This previously unsuspected conformational change may alter the dynamics of Apaf-1, so that ADP can be exchanged for ATP at the other end of the monomer. Thus, a large rotation of the nucleotide binding domain (NBD) and helix domain 1 (HD1) may occur in a concerted manner during cytochrome *c* binding to promote nucleotide exchange. In the absence of pc-9, Apaf-1 conformational changes drive the

Received: December 31, 2012
Revised: March 10, 2013
Published: March 22, 2013

   dx.doi.org/10.1021/bi301721g | *Biochemistry* 2013, 52, 2319−2327

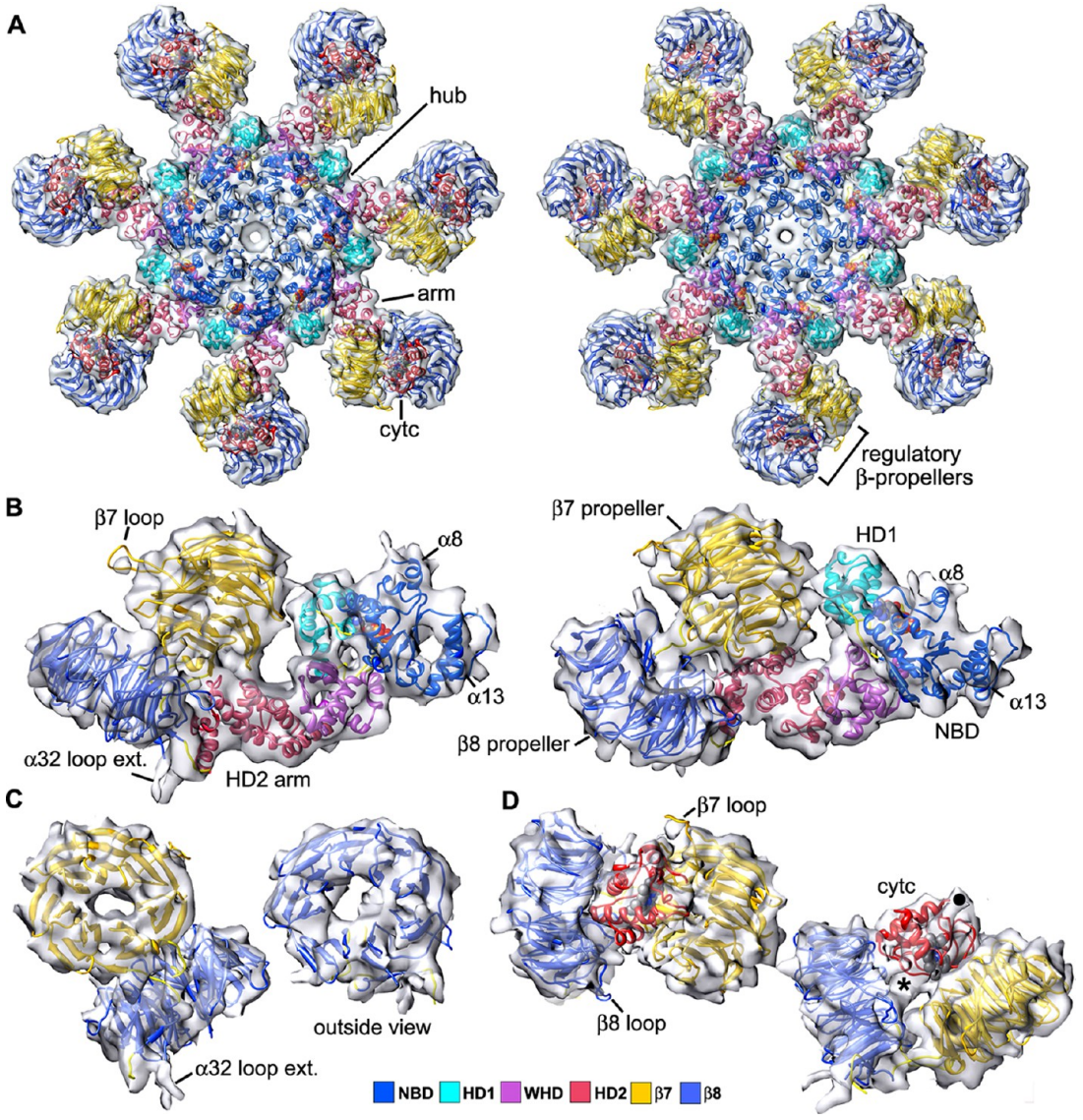

Figure 1. An improved model of the human apoptosome. (A) Top and bottom views are shown of the human apoptosome docked within the electron density at ~9.5 Å resolution. Domains of Apaf-1 are color-coded as indicated. Cytochrome *c* is bound between two *β*-propellers in the regulatory region. (B) The Apaf-1 model is shown in two views, docked within segmented electron density for a single subunit. (C) The fit of 7- and 8-blade *β*-propellers is shown within electron density from the regulatory region. At a higher threshold individual 4-stranded blades of the two *β*-propellers are visible in the density map (not shown) (D) Cytochrome *c* docking between two *β*-propellers is shown in top and side views. Extra density that may arise from the *β*8 loop is indicated with an asterisk. An additional spur of density on cytochrome *c* is marked with a black circle. This density may indicate an alternative position for the short N-terminal helix of bound cytochrome *c*.

assembly of a wheel-like platform with disordered CARDs. However, the Apaf-1 CARD may be accessible in the monomer and thus could interact with a pc-9 CARD, either before or during assembly. Multiple CARD−CARD interactions would then create an acentric disk that converts the apoptosome to an asymmetric proteolysis machine.

MATERIALS AND METHODS

To create an improved model of the apoptosome, we used an electron density map from our previous study with an estimated resolution of ~9.5 Å (EMDB 5186),[19] along with crystal structures of a full length mouse Apaf-1 (pdb id: 3SFZ),[30] a truncated human Apaf-1-591 (pdb id: 1Z6T),[15] and oxidized bovine cytochrome *c* (pdb id: 2B4Z). We started with an existing rigid body model of the human apoptosome (pdb id: 3IZA) that has two generic *β*-propellers. In addition, the apoptosome model deposited in the PDB did not contain cytochrome *c* due to uncertainties in the docking of this small heme protein within the regulatory region in the presence of generic *β*-propellers.

First, we segmented a monomer density from the apoptosome map using the Chimera Segment Map tool.[31] To this end, we zoned around the docked rigid body model of Apaf-1 containing the NBD, HD1, winged helix domain (WHD), helix domain 2 (HD2), two generic *β*-propellers, and a roughly docked cytochrome *c*. We then created human versions of the Apaf-1 *β*-propellers with MODELER using mouse *β*-propellers as templates.[32] These domains, with the exception of cytochrome *c*, were then flexibly docked within the monomer density using Rosetta.[33] In this step, cognate *β*-propellers moved into density and individual helices within the N-terminal half of Apaf-1 also achieved a better fit. Two large

dx.doi.org/10.1021/bi301721g | *Biochemistry* 2013, 52, 2319−2327

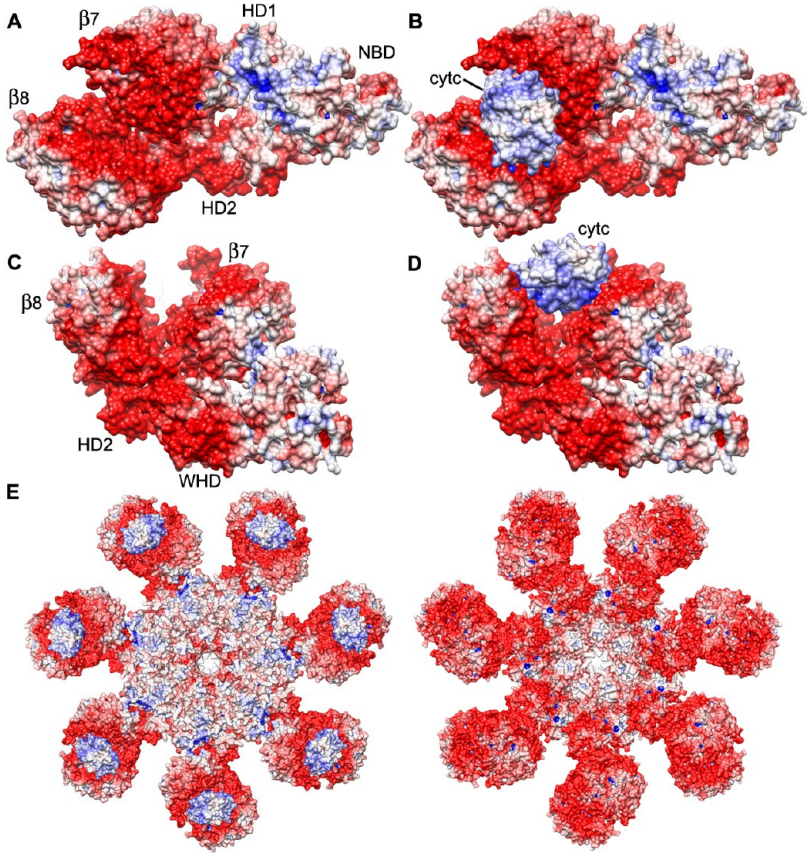

Figure 2. Shape and charge complimentarity are present between β-propellers and cytochrome *c* in the apoptosome. (A) An electrostatic surface representation is shown for the Apaf-1 monomer, as viewed from above the V-shaped groove between the β-propellers. The regulatory region is highly acidic (shown in red). The linear color scale was set from −7 to 7 kcal/mol. (B) Cytochrome *c* is shown bound in the V-shaped groove of the regulatory β-propellers. Note that there is a strong charge complementarity between cytochrome *c* and the V-shaped groove. (C) A side view is shown of the V-shaped groove. (D) A similar view to that in panel C is shown, with bound cytochrome *c*. (E) The electrostatic surface for the entire human apoptosome is shown in top and bottom views to highlight the unusual charge distribution on the platform.

loops that were incomplete in the β-propellers (L788-E795; E1170-T1175) were also created by MODELER and subsequently refined with Rosetta.

The small size of cytochrome *c* and its position between the two β-propellers made this docking more challenging. We roughly docked bovine cytochrome *c* (pdb id: 2B4Z) into one of the monomers' empty densities and zoned around it within 9 Å, making sure that any density attributable to the β-propellers was excluded from this mini-map. Next we used Situs[34] to find the top solution for docking bovine cytochrome *c* into the segmented density. We then retrieved all PDBs identified as cytochrome *c* using the sequence of bovine heart cytochrome c (UniProt number: P62894), within a default cutoff *E*-value of 1 × 10^{-2}. Each of the ∼120 related structures was superimposed onto the initial Situs fit and then fitted locally in the map using Chimera.[31] The top 10 fits based on Chimera's cross-correlation coefficient were then manually inspected, and 2B4Z was selected as the best fit. Starting from different initial positions for local fitting did not result in a higher cross-correlation coefficient.

Finally, a complete apoptosome model with C7 symmetry was generated with Moleman2[35] and molecular contacts in the model were evaluated using PDB validation software. Electrostatic potential surfaces were calculated using APBS.[36] All figures were made by capturing images in Chimera,[31] and subsequent assembly steps were carried out in Adobe Photoshop.

RESULTS

An Improved Model of the Human Apoptosome. A 3D map of the human apoptosome with an Apaf-1 CARD/pc-9 CARD disk was obtained previously at a nominal resolution of ∼9.5 Å, using single particle electron cryo-microscopy.[19] This resolution estimate was based on the quality of fit after rigid body docking of the nucleotide oligomerization domain (NOD) and HD2 arm, combined with an FSC0.5 value of ∼8.5 Å, which overestimated the map resolution.[19] However, atomic structures for the Apaf-1 β-propellers, or closely related templates, were not available for docking into the density. This prevented us from accurately modeling the regulatory region within the apoptosome and precluded a precise docking of cytochrome *c* between β-propellers. Together, the β-propellers and cytochrome *c* account for ∼50% of the mass of the ground-state apoptosome and represent 3 of the 7 ordered domains.

A recent crystal structure of full length mouse Apaf-1[30] allowed us to revisit these issues. Thus, we have now created an improved model of the ground state apoptosome that includes homology models of human β-propellers and bovine cytochrome *c*. Top and bottom views of the final apoptosome model are shown docked within the density map in Figure 1A. The rmsd for Cα atoms within the NOD and HD2 arm is ∼1.3

dx.doi.org/10.1021/bi301721g | *Biochemistry* 2013, 52, 2319−2327

Å for a comparison between rigid and flexibly docked models using all atoms and ligands. Flexible fitting by Rosetta also improved the overall fit within the low pass filtered map (9.5 Å resolution), with a cross-correlation value of 0.939 relative to the rigid body model (0.901).

The quality of the new model in the regulatory region can be seen in a close-up of an Apaf-1 subunit excised from the 3D map (Figure 1B, left and right panels). Individual 7- and 8-blade β-propellers and their linkers are in good density in the regulatory region. The fit was accurate enough to obtain the correct rotational register between β-propellers while maintaining the connectivity of linkers between these domains (Figure 1B,C). However, the novel linker that connects helix α32 of the HD2 arm with the 7- and 8-blade β-propellers remains problematic. Rosetta extended a small helical region in this linker into a full d-strand on the last blade of the 7-blade propeller, and the polypeptide chain then crossed over to form the a-strand of the N-terminal blade of the 8-blade propeller.[30] On the basis of the density map, it is likely that this linker may also form a larger loop between helix α32 in HD2 and the d-strand of the 7-blade propeller. This possibility is indicated by the presence of density for an α32 loop extension that was too fragmented for modeling due to flexibility (Figure 1B,C). The absolute registration of these linker residues with respect to other residues in the map may not be correct, since the map does not have sufficient distinctive features to allow an accurate modeling.

Although loop modeling is only approximate, we found that two extended loops in Apaf-1β-propellers may play important roles in the assembled apoptosome. These loops were partly disordered in the crystal structure.[30] First, a long loop that connects the d-strand of blade 4 with the a-strand of blade 5 in the 7-blade propeller (β7 loop, Figure 1B,D) appears to bend back toward the Y-shaped regulatory region and may interact with cytochrome *c*. Second, a long loop that connects the d-strand of blade 6 with the a-strand of blade 7- in the 8-blade propeller (β8 loop) bends toward the HD2 arm. There is extra density at the base of the V-shaped groove between β-propellers and cytochrome *c*. The β8 loop is long enough to contribute to this feature (unfilled density marked with an asterisk in Figure 1D, right panel).

Once density in the regulatory region was assigned to β-propellers, we docked cytochrome *c* between the β-propellers with Situs (Figures 1C,D and 2). In particular, this docking placed the longest helix of cytochrome *c* in a prominent tubelike density running between the two β-propellers. There are a number of notable features concerning interactions between cytochrome *c* and the β-propellers. First, cytochrome *c* interacts strongly with both β-propellers. Second, the heme group is buried in the interface between cytochrome *c* and the 7-blade propeller and is not very solvent exposed, consistent with earlier measurements.[14] Third, numerous basic residues of cytochrome *c* are present in or near the two interfaces with the β-propellers, including lysine residues 7, 8, 13, 25, 27, 72, 73, and 86−88.[37] Fourth, the calculated electrostatic potential of cytochrome *c* is positive, with the highest potential centered on the heme edge facing the two β-propellers, while the V-shaped groove between β-propellers has an electronegative potential (Figure 2). Finally, the short N-terminal helix of cytochrome *c* may rotate into a new position when bound to the regulatory region (extra density marked with a dot, Figure 1D, right). However, we did not model this reorientation. We surmise that both shape and charge complementarity may play important roles in cytochrome *c* binding to the regulatory β-propellers.

We also determined the overall charge distribution on the apoptosome (excluding the CARDs which are disordered in the ground state).[19] The pattern is quite striking with top and bottom surfaces of the central hub being rather neutral, while β-propellers and the bottom surfaces of the HD2 arm and WHD are electronegative (Figure 2E, top and bottom views). While cytochrome *c* binding partly neutralizes the rather negatively charged regulatory region, large negative patches remain on the bottom of the platform, and this is accentuated by the 7-fold symmetry. Possible biological roles for these strongly negative regions remain to be determined. However, the negative patches could mediate interactions with basic binding sites, including positively charged phospholipid head groups on membrane surfaces. It must also be noted that the charge distribution on the underside of the Apaf-1 apoptosome differs significantly from that shown for the CED-4 apoptosome (see ref 29). Given this discrepancy, we recalculated the charge distribution on the CED-4 apoptosome and found that it too is very electronegative, as suggested by its acidic isoelectric point (not shown). Low calculated PIs for WHD, HD2, and β-propellers of Dark suggest that the fly apoptosome will also have a strongly negative lower surface. Hence, all apoptosomes may share this striking property.

Apaf-1 Conformational Changes during Assembly. An improved model of the human apoptosome and two crystal structures of the Apaf-1 monomer[15,30] allowed us to investigate conformational changes that occur during assembly. To this end, we created a chimeric Apaf-1 monomer with bound ADP, a CARD, and a disordered CARD-NBD linker, by superimposing Apaf-1-591 which contains an N-terminal CARD[15] with mouse Apaf-1 in which the CARD was disordered (Figure 3, left).[30] We compared the Apaf-1 monomer with ADP to the extended conformation with bound ATP in the apoptosome (Figure 3, right), by aligning the two molecules on the central WHD-HD2 module. In this alignment, major conformational

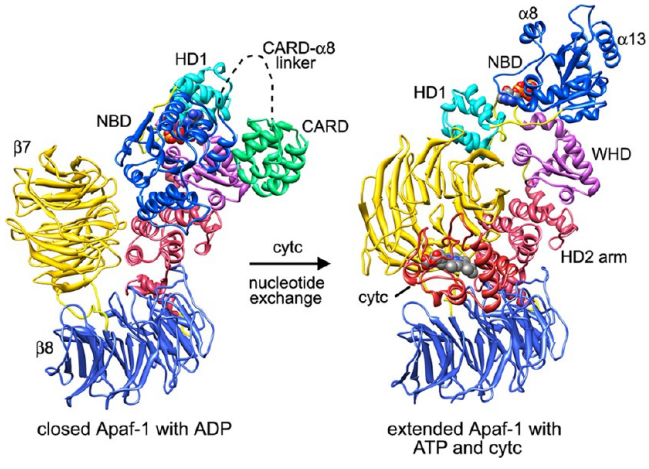

Figure 3. Closed and open conformations of the Apaf-1 subunit. A closed Apaf-1 conformation with bound ADP and an ordered CARD is shown on the left, while an open form of the molecule with bound ATP is shown on the right. A disordered CARD in the assembled conformation of Apaf-1 is not shown. The two Apaf-1 conformations have been aligned on the relatively rigid WHD−HD2 module, which is in the plane of the figure.

changes involve large rotations and translations of domains located at either end of the central WHD−HD2 module.

The rationale for using the crystal structure of full length mouse Apaf-1 as a model for the inactive, ADP conformation is as follows. First, the conformation of the NBD−HD1−WHD region with a buried ADP molecule is nearly identical in crystal structures of human and mouse Apaf-1.[15,30] Second, the WHD−HD2 interface in the central module is extensive and appears to be rather rigid. Third, the interface between the HD2 arm and 8-blade β-propeller is similar in the mouse Apaf-1 crystal structure and in the apoptosome, while the 7-blade β-propeller is in a very different orientation in these two Apaf-1 conformations (see below).

Previous studies have shown that truncated Apaf-1 without β-propellers is constitutively active.[12,38] Hence, it was suggested that β-propellers may regulate accessibility of the N-terminal CARD by shielding this domain from interactions with procaspase-9. Based on our studies, the overall rigidity of the central WHD−HD2 module would probably preclude the β-propellers from directly interacting with the N-terminal CARD. Hence, the regulatory activity of the β-propellers may derive from indirect effects that block Apaf-1 assembly and pc-9 activation.[30]

Since cytochrome *c* triggers assembly, we start with changes in the regulatory region induced by activator binding. Remarkably, only a small translation and rotation of the 8-blade β-propeller occurs relative to the HD2 arm when cytochrome *c* is bound. However, the 7-blade β-propeller undergoes a large twisting motion that brings the inside face of the propeller into proper alignment to form a V-shaped groove, with cytochrome *c* clamped between the two β-propellers (Figure 4A). Thus, cytochrome *c* binding occurs by an induced-fit mechanism that creates the proper binding groove in the regulatory region. The large rotation of the 7-blade β-propeller breaks three salt bridges to HD2 and the NBD that are present in the ADP bound conformation of Apaf-1.[30]

At the N-terminal end of Apaf-1, nucleotide exchange leads to a major reorganization of the NBD−HD1 module, relative to the WHD−HD2 arm, when ADP is replaced by ATP. The NBD−HD1 rearrangement is complicated and can be described in two parts. First, the nucleotide binding module rotates ~180° about the HD1−WHD interface, and during this process, the HD1−WHD loop flips about 60° to interact with ATP (Figure 4B,C).[19,20] The HD1 also rotates about 10° relative to the NBD. These large movements disrupt a salt bridge between His438 in the WHD and the β-phosphate of ADP during nucleotide exchange.[15,30,39] In addition, Arg265 (sensor I) may play a role in nucleotide exchange as this basic side chain appears to stabilize a triad of carboxyl side chains comprised of Asp244, -392, and -439 in the ADP bound conformation of Apaf-1.[30] While we do not have a high resolution view of Apaf-1 with bound ATP, the nucleotide pocket and HD1−WHD loop are similar in CED4. Equivalent arginine residues in the lateral dimer assembly intermediate and the CED4 apoptosome interact with the γ-phosphate of ATP.[29,40] Hence, a rearrangement of the sensor I arginine could favor large conformational changes that occur at the N-terminal end of Apaf-1. Indeed, the inhibitory effect of Ca^{2+} ions on Apaf-1 assembly could be due to cation binding to carboxyl groups in the triad, thereby locking the molecule in the ADP bound form.[41] Helix α8 also moves laterally relative to the NBD to help form the subunit interface in the apoptosome,

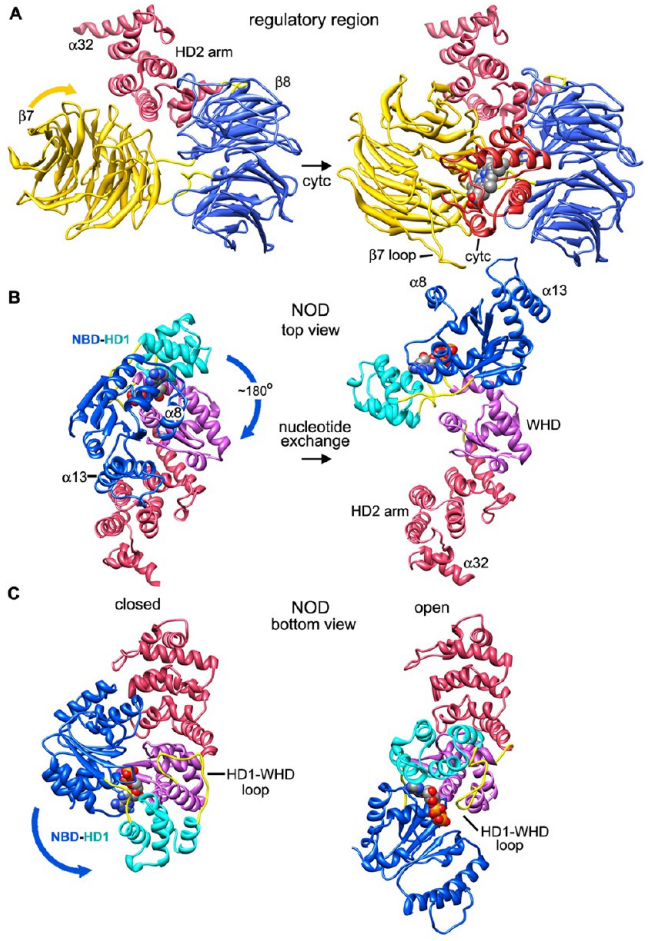

Figure 4. Conformational changes of Apaf-1 during apoptosome assembly. (A) The 7-blade β-propeller twists about 45° toward the reader to form the V-shaped groove, while clamping cytochrome *c* in the regulatory region. Molecules in the two views have been aligned on the HD2 arm. (B) The NBD−HD1 module in the NOD undergoes a large rotation about the HD1−WHD interface during nucleotide exchange and assembly. The direction of view is roughly from above the top surface of the apoptosome. The two views have been aligned on the WHD−HD2 module. (C) A reverse view is shown of the NOD−HD2 region that clearly indicates the rearrangement of the HD1−WHD loop. During this large rotation, the HD1−WHD loop also flips ~60° to interact with bound ATP.

while helices α12 and α13 are positioned to form a picket fence that encircles the central pore during ring assembly.[19]

Based on our studies, apoptosome assembly requires two major conformational changes that occur at either end of the Apaf-1 molecule in response to cytochrome *c* binding and nucleotide exchange (summarized in Figure 5A). However, large scale rotation of the 7-blade β-propeller in the presence of cytochrome *c* results in a significant clash of this domain with the NBD which causes the two domains to interpenetrate (Figure 5B,C). Thus, disruption of salt bridges between the 7-blade β-propeller, HD2, and NBD may predispose the NBD−HD1 module to become more flexible, when coupled with changes in the interface between the 8-blade β-propeller and HD2 arm, and a small flexure of the WHD−HD2 arm. This flexibility may allow the two major conformational changes to occur in a concerted fashion, such that a major clash is avoided.

dx.doi.org/10.1021/bi301721g | *Biochemistry* 2013, 52, 2319−2327

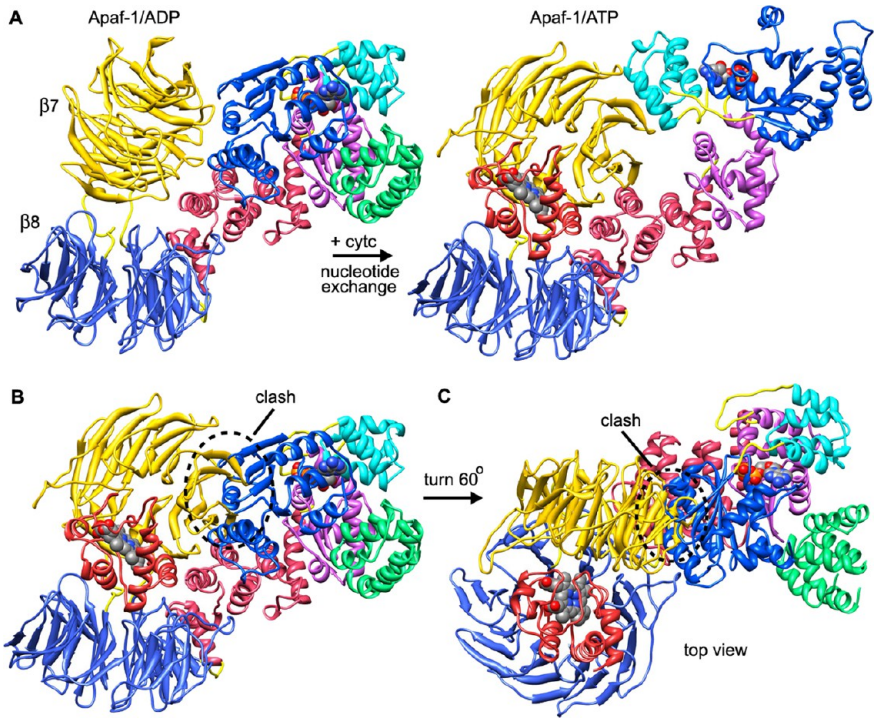

Figure 5. A large clash occurs between the 7-blade β-propeller and the NBD in a simple stepwise reorganization of domains located at either end of the Apaf-1 monomer, during cytochrome *c* binding and nucleotide exchange. (A) Conformations of Apaf-1 are shown in the ADP and ATP bound forms. Cytochrome *c* binding and nucleotide exchange lead to conformational changes at either end of the molecule that promote assembly. (B) Conformational changes must occur in a concerted fashion to avoid a steric clash between the 7-blade β-propeller and NBD (see dashed oval) that would occur upon cytochrome *c* binding. (C) The potential steric clash is shown in a view rotated clockwise by 60° about the arrow indicated.

DISCUSSION

Implications for Apaf-1 Function, Apoptosome Assembly, and pc-9 Activation. Apaf-1 assembly is a critical precondition for pc-9 activation in programmed cell death.[24] Intriguingly, apoptosomes are localized in the proximity of mitochondria ~2 h after induction of cell death in rat pituitary cells and interactions with pc-9 are enhanced.[42] However, Apaf-1 may also have a pro-survival role in which centrosome maturation is regulated.[43] We have shown that Apaf-1 monomers and apoptosomes have an unusual charge distribution with large electronegative surface patches distributed over the WHD, HD2, and β-propellers. This property may be used to target Apaf-1 to nascent centrosomes[43] or to recruit apoptosomes to mitochondria.[42]

Apoptosome assembly and procaspase activation are regulated quite differently in three benchmark metazoans, including humans, flies, and worms.[44] In humans, Apaf-1 is present in healthy cells as an inactive monomer with bound ADP. This conformer of Apaf-1 must bind cytochrome *c* to initiate platform assembly and pc-9 activation (Figure 6). At this point, there is no obvious structural "trigger" that may couple cytochrome *c* binding on one end of the Apaf-1 molecule to nucleotide exchange at the other end. Instead, a series of small changes occur in the interface between the 7-blade β-propeller and NBD/HD2 that may alter the dynamics of Apaf-1 domains so that nucleotide exchange can occur more readily. Indeed, a general loosening of the NBD−HD1−WHD domains must occur for deeply buried ADP to exchange.[15]

The Apaf-1 monomer with bound cytochrome *c* and ATP/dATP is in a more extended conformation that can form lateral intersubunit contacts during apoptosome assembly. Thus, rotation of the NBD−HD1 module frees up important interface surfaces in the NBD so that the innermost ring of NBDs can assemble, with $\alpha12-\alpha13$ helix pairs forming a cylindrical picket fence which encircles the central pore. Movements of the nucleotide binding module (NBD−HD1) also position HD1 to interact with the WHD of an adjacent subunit. The HD1−WHD interaction allows formation of a second ring which encircles the central NBD ring to stabilize the hub. In addition, rotation of the 7-blade β-propeller during cytochrome *c* binding creates the V-shaped regulatory region that extends from the central hub via the HD2 arm (Figure 6, top right). Hence, cytochrome *c* binding appears to proceed via an induced fit mechanism.

In the absence of pc-9, cytochrome *c* and ATP/dATP bind to Apaf-1 to initiate assembly of the ground state apoptosome in which CARDs are flexibly tethered via CARD−NBD linkers to the platform.[19,45] Since the CARD−NBD linker is disordered in the ADP bound conformation of Apaf-1 and the CARD is exposed,[15] an Apaf-1 monomer may interact with pc-9 through homotypic CARD−CARD interactions, either before or during assembly (Figure 6, top). In fact, pc-9 promotes nucleotide exchange and pc-9 activation.[13] However, an interaction between Apaf-1 and pc-9 monomers would not be sufficient to activate pc-9 in the absence of platform assembly.

The end product of Apaf-1 and pc-9 coassembly is an asymmetric proteolytic machine containing activated pc-9. In this complex, the CARD−CARD disk is acentrically positioned on the heptameric platform (Figure 6, bottom).[45] Currently, the structure of this disklike feature remains mysterious. However, CARDs are members of the Death Domain superfamily of 6-helix bundle proteins that form activation platforms, in which interacting DD pairs form short helical stacks or lock washer like disks.[46−48] Thus, a disk comprised of

dx.doi.org/10.1021/bi301721g | *Biochemistry* 2013, 52, 2319−2327

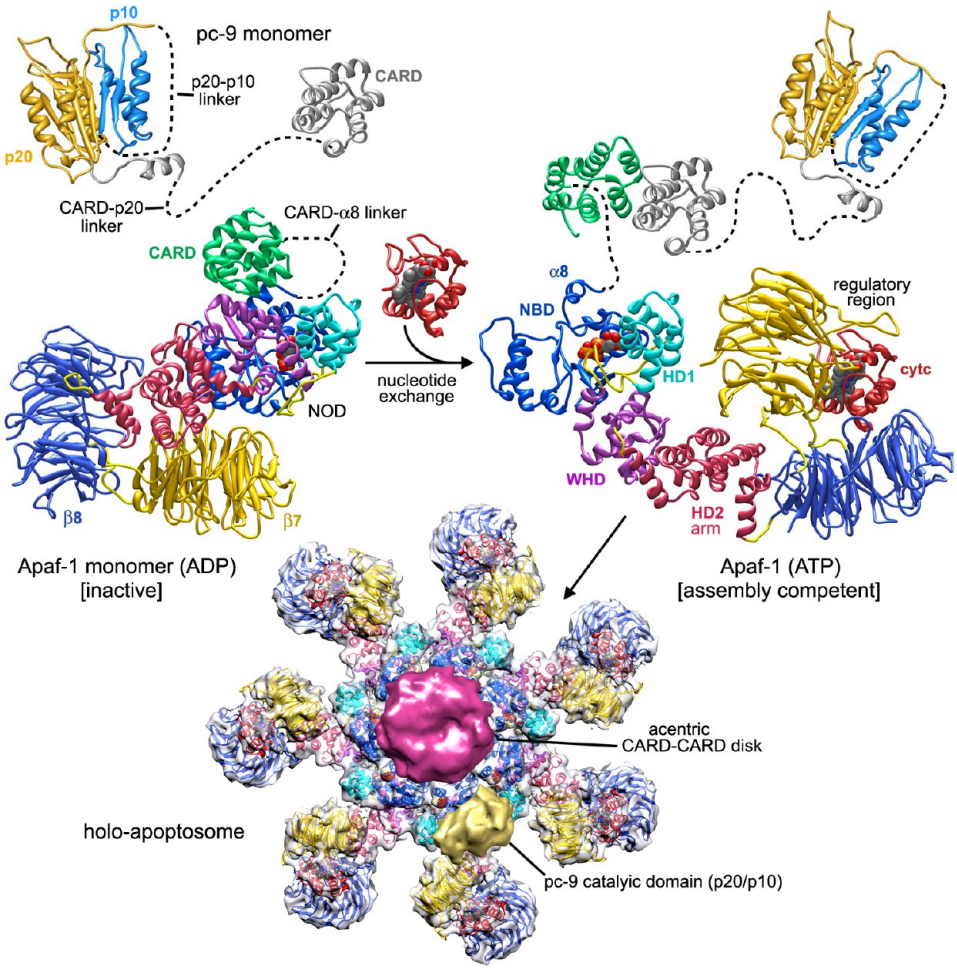

Figure 6. Apaf-1 assembly and formation of the holo-apoptosome. A composite model is shown for apoptosome assembly and pc-9 activation that incorporates known structures and interactions in the pathway (see text for details). Linkers play important roles and are indicated with dashed lines. Since the Apaf-1 CARD is accessible, it may form a complex with pc-9 either before or during apoptosome assembly, resulting in the formation of a holo-apoptosome with an acentric CARD−CARD disk (shown as a magenta surface). This disk is probably larger in diameter but its size may have been reduced due to a limited flexibility. The model for the holo-apoptosome is a composite derived from two recently determined structures.[19,20] A pc-9 catalytic domain comprised of p20/p10 subunits is shown as a gold surface bound to an NBD in the central hub.

Apaf-1 and pc-9 CARDs may not follow the cylindrical symmetry of the apoptosome. In fact, the disk has an asymmetric and somewhat tilted structure in 3D maps of apoptosomes with pc-9 or pc-9 CARDs that are calculated without imposing 7-fold rotational symmetry.[45] Critically the CARD−CARD disk serves to anchor pc-9 catalytic domains in close proximity to the platform. The acentric orientation and size of the disk may block possible binding sites for pc-9 catalytic domains on the central hub. In this model, an acentric CARD−CARD disk would serve as a spatial filter that blocks many of the potential binding sits on the central hub, leaving only one site available to bind and activate pc-9 (Figure 6, bottom).[44,45]

■ CONCLUSIONS

We have provided a greatly improved 3D model of the human apoptosome that contains the N-terminal NOD, HD2, cognate β-propellers, and cytochrome *c*. This model allowed us to describe conformational changes in Apaf-1. In particular, cytochrome *c* binding to regulatory β-propellers is probably guided by an induced-fit mechanism and charge complementarity.[14] These conformational changes lead to nucleotide exchange and formation of a more extended Apaf-1 monomer that is competent to assemble. Strikingly, Apaf-1 may coassemble in the presence of pc-9 to form a functional holo-apoptosome.[13] Further studies are needed to reveal platform and CARD−CARD disk assembly at higher resolution and to clarify the mechanism of pc-9 activation.

■ ASSOCIATED CONTENT

Accession Codes

Coordinates for the revised human apoptosome model have been deposited in the Protein Data Bank (pdb code: 3J2T).

■ AUTHOR INFORMATION

Corresponding Author

*E-mail cakey@bu.edu; Ph 617 638 4051.

Funding

This work was supported by a grant from the NIH to C.W.A. (R01 GM63834). M.T. is supported partly by an MRC Centenary Award (G0600084).

Notes

The authors declare no competing financial interest.

■ ACKNOWLEDGMENTS

We thank Frank DiMaio for helpful discussions on flexible fitting with Rosetta.

■ ABBREVIATIONS

Apaf-1, apoptosis protease activation factor 1; pc-9, procaspase-9; CARD, caspase activation and recruitment domain; NOD, nucleotide oligomerization domain; NBD, nucleotide binding domain; HD1, helical domain 1; WHD, winged helix domain; HD2, helical domain 2; ATP, adenosine triphosphate; ADP, adenosine diphosphate.

■ REFERENCES

(1) Green, D. R., and Evan, G. I. (2002) A matter of life and death. *Cancer Cell 1*, 19−30.
(2) Song, Z., and Steller, H. (1999) Death by design: mechanism and control of apoptosis. *Trends Cell Biol. 12*, 49−52.
(3) Salvesen, G. S., and Dixit, V. M. (1997) Caspases: intracellular signaling by proteolysis. *Cell 91*, 443−446.
(4) Danial, N. N., and Korsmeyer, S. J. (2004) Cell death: critical control points. *Cell 116*, 205−219.
(5) Thompson, C. B. (1995) Apoptosis in the pathogenesis and treatment of disease. *Science 267*, 1456−1462.
(6) Liu, X., Kim, C. N., Yang, J., Jemmerson, R., and Wang, X. (1996) Induction of apoptotic program in cell free extracts: requirement for dATP and cytochrome c. *Cell 86*, 147−157.
(7) Li, P., Nijhawan, D., Budihardjo, I., Srinivasula, S. M., Ahmad, M., Alnemri, E. S., and Wang, X. (1997) Cytochrome c and dATP-dependent formation of Apaf-1/Caspase-9 complex initiates an apoptotic protease cascade. *Cell 91*, 479−489.
(8) Gonzalvez, F., and Gottlieb, E. (2007) Cardiolipin: setting the beat of apoptosis. *Apoptosis 12*, 877−885.
(9) Tait, S. W., and Green, D. R. (2010) Mitochondria and cell death: outer membrane permeabilization and beyond. *Nat. Rev. Mol. Cell Biol. 11*, 621−632.
(10) Hu, Y., Benedict, M. A., Ding, L., and Nunez, G. (1999) Role of Cytochrome c and dATP/ATP hydrolysis in Apaf-1 mediated caspase-9 activation and apoptosis. *EMBO J. 13*, 3586−3595.
(11) Zou, H., Li, Y., Liu, X., and Wang, X. (1999) An Apaf-1 cytochrome c multimeric complex is a functional apoptosome that activates procaspase-9. *J. Biol. Chem. 274*, 11549−11556.
(12) Srinivasula, S. M., Ahmad, M., Fernandes-Alnemri, T., and Alnemri, E. S. (1998) Autoactivation of procaspase-9 by Apaf-1 mediated oligomerization. *Mol. Cell 1*, 949−957.
(13) Jiang, X., and Wang, X. (2000) Cytochrome c promotes caspase-9 activation by inducing nucleotide binding to Apaf-1. *J. Biol. Chem. 275*, 31199−31203.
(14) Purring-Koch, C., and McLendon, G. (2000) Cytochrome c binding to Apaf-1: the effects of dATP and ionic strength. *Proc. Natl. Acad. Sci. U. S. A. 97*, 11928−11931.
(15) Riedl, S. J., Li, W., Chao, Y., Schwarzenbacher, R., and Shi, Y. (2005) Structure of the apoptotic protease-activating factor 1 bound to ADP. *Nature 434*, 926−933.
(16) Reubold, T. F., Wohlgemuth, S., and Eschenburg, S. (2009) A new model for the transition of APAF-1 from inactive monomer to caspase-activating apoptosome. *J. Biol. Chem. 284*, 32717−32724.
(17) Acehan, D., Jiang, X., Morgan, D. G., Heuser, J. E., Wang, X., and Akey, C. W. (2002) Three-dimensional structure of the apoptosome: implications for assembly, procaspase-9 binding and activation. *Mol. Cell 9*, 423−432.
(18) Yu, X., Acehan, D., Menetret, J. F., Booth, C. R., Ludtke, S. J., Riedl, S. J., Shi, Y., Wang, X., and Akey, C. W. (2005) A structure of the human apoptosome at 12.8 Å resolution provides insights into this cell death platform. *Structure 13*, 1725−1735.
(19) Yuan, S., Yu, X., Topf, M., Ludtke, S. J., Wang, X., and Akey, C. W. (2010) Structure of an apoptosome-procaspase-9 CARD complex. *Structure 18*, 571−583.
(20) Yuan, S., Yu, X., Topf, M., Dorstyn, L., Kumar, S., Ludtke, S. J., and Akey, C. W. (2011) Structure of the *Drosophila* apoptosome at 6.9 Å resolution. *Structure 19*, 128−140.
(21) Zou, H., Henzel, W. J., Liu, X., Lutschg, A., and Wang, X. (1997) Apaf-1, a human protein homologous to C. elegans CED-4, participates in cytochrome c dependent activation of caspase-3. *Cell 90*, 405−413.
(22) Rodriguez, J., and Lazebnik, Y. (1999) Caspase-9 and Apaf-1 form an active holoenzyme. *Genes Dev. 13*, 3179−3184.
(23) Yin, Q., Park, H. H., Chung, J. Y., Lin, S. C., Lo, Y. C., da Graca, L. S., Jiang, X., and Wu, H. (2006) Caspase-9 holoenzyme is a specific and optimal procaspase-3 processing machine. *Mol. Cell 22*, 259−268.
(24) Bratton, S. B., and Salvesen, G. S. (2010) Regulation of the Apaf-1-caspase-9 apoptosome. *J. Cell. Sci. 123*, 3209−3214.
(25) Renatus, M., Stennicke, H. R., Scott, F. L., Liddington, R. C., and Salvesen, G. S. (2001) Dimer formation drives the activation of the cell death protease caspase-9. *Proc. Natl. Acad. Sci. U. S. A. 98*, 14250−14255.
(26) Pop, C., Timmer, J., Sperandio, S., and Salvesen, G. S. (2006) The apoptosome activates caspase-9 by dimerization. *Mol. Cell 22*, 269−275.
(27) Boatright, K. M., Renatus, M., Scott, F. L., Sperandio, S., Shin, H., Pedersen, I. M., Ricci, J. E., Edris, W. A., Sutherlin, D. P., Green, D. R., and Salvesen, G. S. (2003) A unified model for apical caspase activation. *Mol. Cell 11*, 529−541.
(28) Chao, Y., Shiozaki, E. N., Srinivasula, S. M., Rigotti, D. J., Fairman, R., and Shi, Y. (2005) Engineering a dimeric caspase-9: a re-evaluation of the induced proximity model for caspase activation. *PLoS Biol. 3* (6), e183.
(29) Qi, S., Pang, Y., Hu, Q., Liu, Q., Li, H., Zhou, Y., He, T., Liang, Q., Liu, Y., Yuan, X., Luo, G., Li, H., Wang, J., Yan, N., and Shi, Y. (2010) Crystal Structure of the *Caenorhabditis elegans* apoptosome reveals an octameric assembly of CED-4. *Cell 141*, 446−457.
(30) Reubold, T. F., Wohlgemuth, S., and Eschenburg, S. (2011) Crystal structure of full-length Apaf-1: how the death signal is relayed in the mitochondrial pathway of apoptosis. *Structure 19*, 1074−1083.
(31) Goddard, T. D., Huang, C. C., and Ferrin, T. E. (2005) Software extensions to UCSF chimera for interactive visualization of large molecular assemblies. *Structure 13*, 473−482.
(32) Sali, A., and Blundell, T. L. (1993) Comparative protein modelling by satisfaction of spatial restraints. *J. Mol. Biol. 234*, 779−815.
(33) DiMaio, F., Tyka, M. D., Baker, M. L., Chiu, W., and Baker, D. (2009) Refinement of protein structures into low-resolution density maps using rosetta. *J. Mol. Biol. 392*, 181−190.
(34) Wriggers, W. (2010) Using Situs for the integration of multi-resolution structures. *Biophys. Rev. 2*, 21−27.
(35) Kleywegt, G. J. Unpublished program, Uppsala University, Uppsala, Sweden.
(36) Baker, N. A., Sept, D., Joseph, S., Holst, M. J., and McCammon, J. A. (2001) Electrostatics of nanosystems: application to microtubules and the ribosome. *Proc. Natl. Acad. Sci. U. S. A. 98*, 10037−10041.
(37) Yu, T., Wang, X., Purring-Koch, C., Wei, Y., and McLendon, G. L. (2001) A mutational epitope for cytochrome C binding to the apoptosis protease activation factor-1. *J. Biol. Chem. 276*, 13034−13038.
(38) Hu, Y., Ding, L., Spencer, D. M., and Núñez, G. (1998) WD-40 repeat region regulates Apaf-1 self-association and procaspase-9 activation. *J. Biol. Chem. 273*, 33489−33494.
(39) Danot, O., Marquenet, E., Vidal-Ingigliardi, D., and Richet, E. (2009) Wheel of life, wheel of death: a mechanistic insights into signaling by STAND proteins. *Structure 17*, 172−182.
(40) Yan, N., Chai, J., Lee, E. S., Gu, L., Liu, Q., He, J., Wu, J. W., Kokel, D., Li, H., Hao, Q., Xue, D., and Shi, Y. (2005) Structure of the CED-4-CED-9 complex provides insights into programmed cell death in Caenorhabditis elegans. *Nature 437*, 831−837.
(41) Bao, Q., Lu, W., Rabinowitz, J. D., and Shi, Y. (2007) Calcium blocks formation of apoptosome by preventing nucleotide exchange in Apaf-1. *Mol. Cell 25*, 181−192.

(42) Potokar, M., Kreft, M., Chowdhury, H. H., Vardjan, N., and Zorec, R. (2006) Subcellular localization of Apaf-1 in apoptotic rat pituitary cells. *Am. J. Physiol. Cell Physiol. 290*, C672−677.
(43) Ferraro, E., Pesaresi, M. G., De Zio, D., Cencioni, M. T., Gortat, A., Cozzolino, M., Berghella, L., Salvatore, A. M., Oettinghaus, B., Scorrano, L., Pérez-Payà, E., and Cecconi, F. (2011) Apaf1 plays a pro-survival role by regulating centrosome morphology and function. *J. Cell Sci. 124*, 3450−3463.
(44) Yuan, S.; Akey, C. W. Apoptosomes: structure, assembly and procaspase activation. *Structure*, submitted.
(45) Yuan, S., Yu, X., Asara, J. M., Heuser, J. E., Ludtke, S. J., and Akey, C. W. (2011) The holo-apoptosome: activation of procaspase-9 and interactions with procaspase-3. *Structure 19*, 1084−1096.
(46) Park, H. H., Logette, E., Raunser, S., Cuenin, S., Walz, T., Tschopp, J., and Wu, H. (2007) Death domain assembly mechanism revealed by crystal structure of the oligomeric PIDDosome core complex. *Cell 128*, 533−546.
(47) Park, H. H., Lo, Y. C., Lin, S. C., Wang, L., Yan,g, J. K., and Wu, H. (2007) The death domain superfamily in intracellular signaling of apoptosis and inflammation. *Annu. Rev. Immunol. 25*, 561−586.
(48) Wang, L., Yang, J. K., Kabaleeswaran, V., Rice, A. J., Cruz, A. C., Park, A. Y., Yin, Q., Damko, E., Jang, S. B., Raunser, S., Robinson, C. V., Siegel, R. M., Walz, T., and Wu, H. (2010) The Fas-FADD death domain complex structure reveals the basis of DISC assembly and disease mutations. *Nat. Struct. Mol. Biol. 17*, 1324−1329.